

Strong Proquinoidal Acceptor Enables High-Performance Ambipolar Organic Electrochemical Transistors

Xiran Pan, Zhibo Ren, Yiheng Chen, Yuting Zheng, Peiyun Li, Wenxi Sun, Jingcao Xu, Ju-Peng Chen, Gao-Yang Ge, Qi Li, Zhiyuan Xiong, Zhi Zhang, Rong Zhu, Yu-Qing Zheng, and Ting Lei*

Ambipolar organic electrochemical transistors (OECTs) can simplify manufacturing processes and reduce device footprints, yet their performance still lags behind their p-type and n-type counterparts due to limited molecular design strategies. Here, incorporating strong proquinoidal building blocks effectively addresses this challenge is demonstrated. Using a computational acceptor screening approach, three TBDOPV-based polymers are designed and synthesized: P(bgTBDOPV-T), P(bgTBDOPV-EDOT), and P(bgTBDOPV-MeOT2), all exhibiting ambipolar behavior across various donor moieties. Remarkably, P(bgTBDOPV-EDOT) achieves record-high figure-of-merit (μC^*) values, reaching $268 \text{ F cm}^{-1} \text{ V}^{-1} \text{ s}^{-1}$ for p-type and $107 \text{ F cm}^{-1} \text{ V}^{-1} \text{ s}^{-1}$ for n-type operations. Additionally, P(bgTBDOPV-EDOT) exhibits low operation voltages ($V_{\text{Th,p}} = -0.55 \text{ V}$ and $V_{\text{Th,n}} = 0.32 \text{ V}$), with fast response times ($\tau_{\text{on}}/\tau_{\text{off}} = 0.48/0.36 \text{ ms}$ for p-type and $0.41/0.41 \text{ ms}$ for n-type) and enhanced operational stability. Inverter devices based on P(bgTBDOPV-EDOT) show high voltage gains of 173 V/V . Theoretical calculations and data analysis confirm that strong proquinoidal acceptors significantly enhance the delocalization of both positive and negative polarons, offering an effective pathway for higher-performance ambipolar OECT materials.

operate in aqueous environments.^[4] The construction of p-n complementary logic circuits enhances OECT functionality. In biosensing, these circuits enable real-time, high-sensitivity ion detection.^[5] In neural interfaces, they amplify signals^[6] and improve common-mode rejection.^[7] In neuromorphic electronics, they support several neuronal characteristics like ion-modulated spiking.^[8] Building complementary n-type and p-type circuits requires two separate material patterning steps, increasing manufacturing complexity and cost. Ambipolar materials, which can transport both holes and electrons, reduce manufacturing complexity by enabling logic circuits with a single polymer patterning step.^[9] Circuits built with ambipolar materials could potentially deliver performance comparable to traditional p-n complementary circuits.^[10] By utilizing cofacial vertical designs, ambipolar OECTs can reduce device footprints and increase transistor density.^[11] Recently, ambipolar OECT-based inverters have demonstrated a voltage-regulated

1. Introduction

Organic electrochemical transistors (OECTs) show significant potential in biochemical sensors,^[1] neural interfaces,^[2] and neuromorphic electronics^[3] due to their low operating voltage, high transduction, good biocompatibility, and capability to

dual mode: volatile receptor and nonvolatile synapse, highlighting their potential for neuromorphic computing applications.^[12]

However, the performance of ambipolar OECTs still lags far behind that of the unipolar materials. Although blending n-type and p-type materials has successfully achieved ambipolar OECTs with a p-type μC^* of $22.8 \text{ F cm}^{-1} \text{ V}^{-1} \text{ s}^{-1}$ and an n-type

X. Pan, Z. Ren, Y. Chen, Y. Zheng, P. Li, W. Sun, J. Xu, J.-P. Chen, G.-Y. Ge, Q. Li, Z. Xiong, Z. Zhang, T. Lei
 National Key Laboratory of Advanced Micro and Nano Manufacture Technology
 Key Laboratory of Polymer Chemistry and Physics of Ministry of Education
 School of Materials Science and Engineering
 Peking University
 Beijing 100871, P. R. China
 E-mail: tinglei@pku.edu.cn

R. Zhu
 Beijing National Laboratory of Molecular Sciences (BNLMS)
 Key Laboratory of Bioorganic Chemistry and Molecular Engineering of Ministry of Education
 College of Chemistry and Molecular Engineering
 Peking University
 Beijing 100871, P. R. China
 Y.-Q. Zheng
 National Key Laboratory of Advanced Micro and Nano Manufacture Technology
 Beijing Advanced Innovation Center for Integrated Circuits
 School of Integrated Circuits
 Peking University
 Beijing 100871, P. R. China

The ORCID identification number(s) for the author(s) of this article can be found under <https://doi.org/10.1002/adma.202417146>

DOI: 10.1002/adma.202417146

μC^* of $11.8 \text{ F cm}^{-1} \text{ V}^{-1} \text{ s}^{-1}$,^[13] blending often leads to phase separation and non-uniform film morphologies, complicating large-area fabrication. Single-component ambipolar materials offer greater potential by simplifying processing and ensuring uniform films. Conventional wisdom suggests that a low LUMO level promotes electron transport, while a high HOMO level supports hole transport, making narrow-band gap polymers key to ambipolar performance. Donor-acceptor (D-A) copolymers, particularly NDI-based ones, are often used to achieve this, as their orbital coupling narrows the bandgap, enabling both *p*-type and *n*-type carrier injection.^[14] However, few D-A copolymers exhibit ambipolar behaviors in OECTs, and their performance remains limited. DPP-based copolymers have achieved relatively high μC^* values^[9,12]; however, they typically require higher operating voltages, leading to significant side reactions and reduced device stability.^[15] Furthermore, these high operating voltages hinder the development of low-power electronics. Recently, a BDOPV-based D-A polymer, DHF-gTT, achieved more balanced properties.^[16] Nevertheless, these materials still fall significantly short of their unipolar counterparts. To date, issues such as low μC^* , high operating voltage, and poor stability restrict the application of ambipolar OECTs, highlighting the need for alternative design strategies to enhance ambipolar performance.

In this work, we achieved high-performance ambipolar OECTs by introducing a strong proquinoidal acceptor. Using density functional theory (DFT) calculations, we identified the thiophene-fused benzodifurandione-based oligo(*p*-phenylenevinylene) (TBDOPV),^[17] a strong proquinoidal acceptor. We paired it with various donors to create ambipolar OECT materials. Adjusting the electron-donating strength of the donor moiety enabled us to fine-tune both *p*-type and *n*-type performance. Notably, P(bgTBDOPV-EDOT) displayed relatively balanced and stable *p*-type and *n*-type characteristics, with a *p*-type μC^* of $268 \text{ F cm}^{-1} \text{ V}^{-1} \text{ s}^{-1}$ and an *n*-type μC^* of $107 \text{ F cm}^{-1} \text{ V}^{-1} \text{ s}^{-1}$, which are both the state-of-art among ambipolar OECT materials. Furthermore, we fabricated inverters through a one-step polymer patterning process, achieving a maximum gain of 173 V/V. We demonstrate that the proquinoidal building block effectively narrows the bandgap, and more importantly, enhances the delocalization of both positive and negative polarons, leading to high hole and electron mobilities and outstanding ambipolar performance. Our work highlights the great potential of incorporating strong proquinoidal building blocks for high-performance ambipolar material design.

2. Results and Discussion

2.1. Polymer Synthesis and Characterization

As noted above, achieving ambipolarity requires the polymer to have a high HOMO level and a low LUMO level, indicating a narrow bandgap characteristic. Besides constructing D-A structures, enhancing the quinoidal character of π -conjugated systems is also an effective approach to obtaining a narrow bandgap. Incorporating proquinoidal building blocks can effectively enhance the polymer's quinoidal character. We used DFT calculations to

select a strong proquinoidal building block. Polymers with strong quinonoid resonance typically favor high-spin triplet states over singlet states. The energy difference between the singlet and triplet states, ΔE_{ST} ($\Delta E_{\text{ST}} = E_{\text{S}} - E_{\text{T}}$), can be used for screening proquinoidal building blocks.^[18] A larger ΔE_{ST} signifies a more favorable triplet state, reflecting stronger proquinoidal features.^[19] Consequently, TBDOPV was chosen as the polymer's acceptor due to its minimal $|\Delta E_{\text{ST}}|$ (Figure 1a), indicating a potentially strong proquinoidal electronic structure in TBDOPV-based copolymers (Figure 1b).

Figure 1c illustrates the synthetic routes for the three polymers. TBDOPV has a rigid planar structure, leading to strong intermolecular interactions and low solubility. To increase its solubility, we introduced branched ethylene glycol side chains (R) to TBDOPV. The R branches extend further from the core to reduce the π - π stacking distance, which may enhance charge carrier mobility.^[20] By conjugating TBDOPV with three types of donors, thiophene (T), 3,4-ethylenedioxythiophene (EDOT), and 3,3'-dimethoxy-2,2'-bithiophene (MeOT2), we synthesized a series of copolymers: P(bgTBDOPV-T), P(bgTBDOPV-EDOT), and P(bgTBDOPV-MeOT2). The electron-donating ability of these donors increases progressively. All polymers were obtained via Pd-catalyzed Stille coupling reactions, purified by Soxhlet extraction and finally collected by hexafluoroisopropanol (HFIP). The synthetic details can be found in the Supporting Information. The molecular weights of the polymers were evaluated by gel permeation chromatography (GPC) using HFIP as the eluent: $M_w/M_n = 38.1/18.9$ kDa for P(bgTBDOPV-T), $M_w/M_n = 47.2/23.4$ kDa for P(bgTBDOPV-EDOT), and $M_w/M_n = 45.2/22.5$ kDa for P(bgTBDOPV-MeOT2) (Figure S1, Supporting Information). Based on the thermogravimetric analysis (TGA) (Figures S2 and S3, Supporting Information), the degradation temperatures at 5% weight loss were found to be 263, 213, and 222 °C for P(bgTBDOPV-T), P(bgTBDOPV-EDOT), and P(bgTBDOPV-MeOT2), respectively, suggesting good thermal stability of the three polymers.

The optoelectronic properties of the three polymers were characterized by UV-vis-NIR absorption spectra and cyclic voltammetry (CV) (Figure 2a–c; Table S1, Supporting Information). All polymers exhibited typical intramolecular charge transfer (ICT) in the low-energy region (Figure 2a,b).^[21] The maximum absorption peaks of P(bgTBDOPV-T), P(bgTBDOPV-EDOT), and P(bgTBDOPV-MeOT2) gradually redshift (Figure 2a,b) due to the increased donor electron density and enhanced ICT.^[22] The maximum absorption peaks of all the polymer films blue-shifted compared to their dilute solution state (Figure S4, Supporting Information), largely due to the influence of the polar solvent, which could stabilize the excited charge transfer states. The measured ionization potentials (IP) and electron affinities (EA) of P(bgTBDOPV-T), P(bgTBDOPV-EDOT), and P(bgTBDOPV-MeOT2) are 5.18/4.26, 4.92/4.19, and 4.61/4.05 eV, respectively (Figure 2c), with corresponding CV bandgaps of 0.92, 0.73, and 0.56 eV. These results indicate that a strong electron-donating donor can raise energy levels and narrow the bandgap, consistent with the DFT calculations (Figure S8a, Supporting Information). All three polymers exhibit narrow bandgaps below 1 eV, demonstrating the potential of TBDOPV for ambipolar materials.

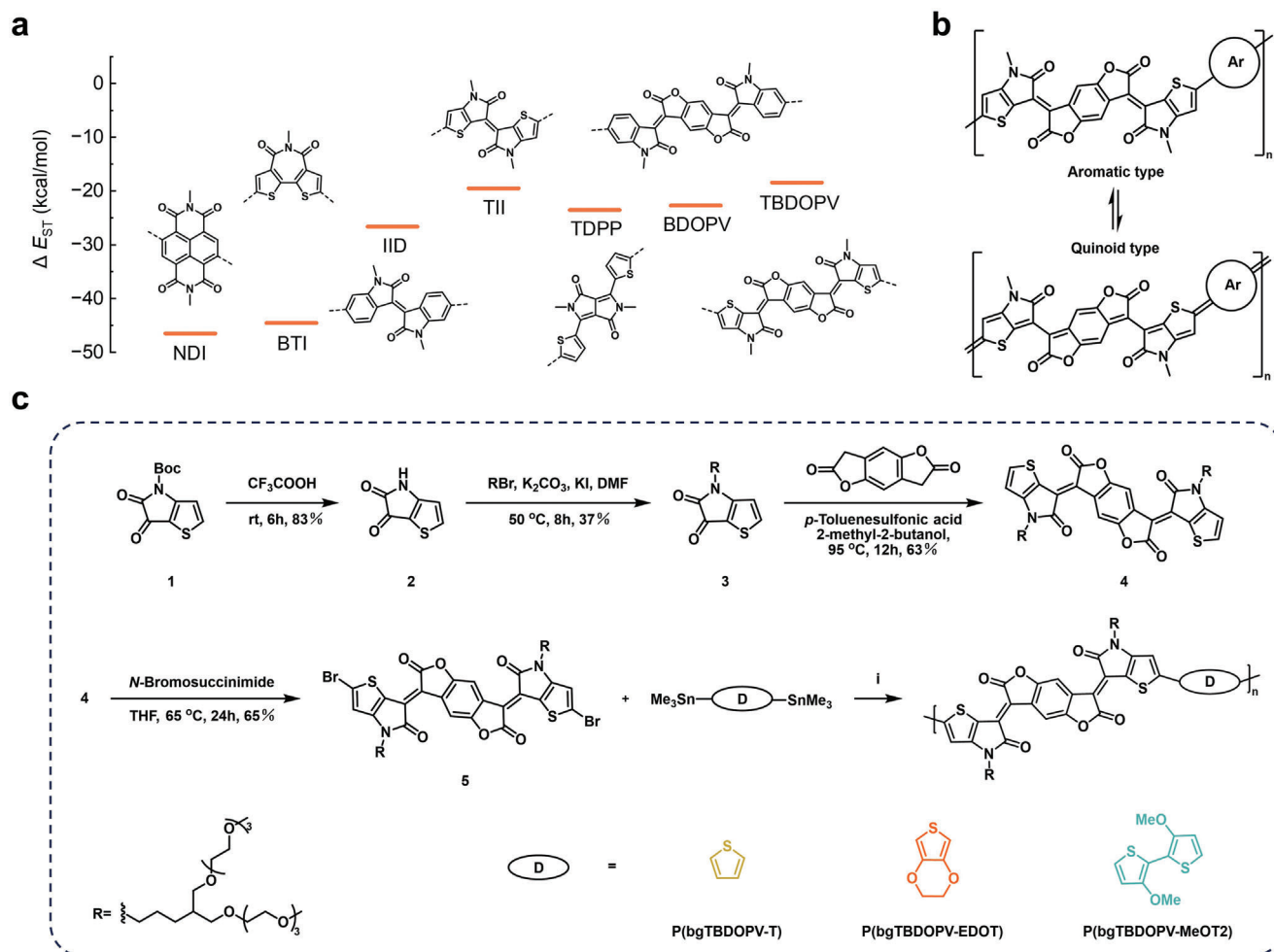


Figure 1. a) Calculated ΔE_{ST} values of seven commonly used acceptors. b) Aromatic and quinoidal structures of the TBDOPV-based polymers. c) Synthetic routes to the three polymers: P(bgTBDOPV-T), P(bgTBDOPV-EDOT), and P(bgTBDOPV-MeOT2). Conditions: (i) $Pd(PPh_3)_4, CuI, DMF/CB$ for P(bgTBDOPV-T), P(bgTBDOPV-EDOT); $Pd(PPh_3)_4$ and o -xylene for P(bgTBDOPV-MeOT2).

2.2. OECT Device Fabrication and Characterization

All the OECT devices were fabricated by a photolithography and perylene patterning method. The semiconducting layer was deposited by spin-coating the HFIP solutions of the three polymers (see Supporting Information for more details). The following equation (Equation 1), based on the Bernards' model,^[23] was used to evaluate the performance of polymers:

$$g_m = \left(\frac{W}{L}\right) \cdot d \cdot \mu \cdot C^* \cdot |(V_{Th} - V_{GS})| \quad (1)$$

where g_m is the transconductance in the saturation regime; W , L , and d are the channel width, length, and film thickness, respectively; μ denotes the charge carrier mobility; C^* denotes the capacitance of the channel per unit volume; V_{Th} is the threshold voltage; and V_{GS} is the voltage between the gate and source electrodes.

All three polymers displayed typical ambipolar characteristics (Figure 3a–f, Table 1). P(bgTBDOPV-T), with its relatively weaker donor, faced difficulty in anion injection, leading to a high p -type threshold voltage ($V_{Th,p}$) of -0.72 V and poor p -type cycling stability (Figure S12c, Supporting Information). These results indicate that the thiophene segment is insufficient to maintain a stable positively charged polaron. In comparison, P(bgTBDOPV-EDOT) exhibited relatively balanced ambipolar performance with p -type and n -type μC^* of 268 and 107 $F\text{ cm}^{-1}\text{ V}^{-1}\text{ s}^{-1}$, respectively (Figure 3i). Meanwhile, P(bgTBDOPV-EDOT) showed high $g_{m,norm}$ of 88.3 and 34.8 $S\text{ cm}^{-1}$ for p -type and n -type, respectively, demonstrating remarkable amplification ability as a sensor. Among the three, MeOT2 is the most electron-rich donor, making P(bgTBDOPV-MeOT2) have the lowest $V_{Th,p}$ of -0.29 V. P(bgTBDOPV-MeOT2) showed a p -type μC^* of 234 $F\text{ cm}^{-1}\text{ V}^{-1}\text{ s}^{-1}$ and a $g_{m,norm}$ of 108 $S\text{ cm}^{-1}$. However, the n -type performance of P(bgTBDOPV-MeOT2) is significantly hindered by its strong donor, resulting in the lowest n -type performance with a μC^* value of 68.7 $F\text{ cm}^{-1}\text{ V}^{-1}\text{ s}^{-1}$. Due to their high HOMO and low LUMO energy levels, both

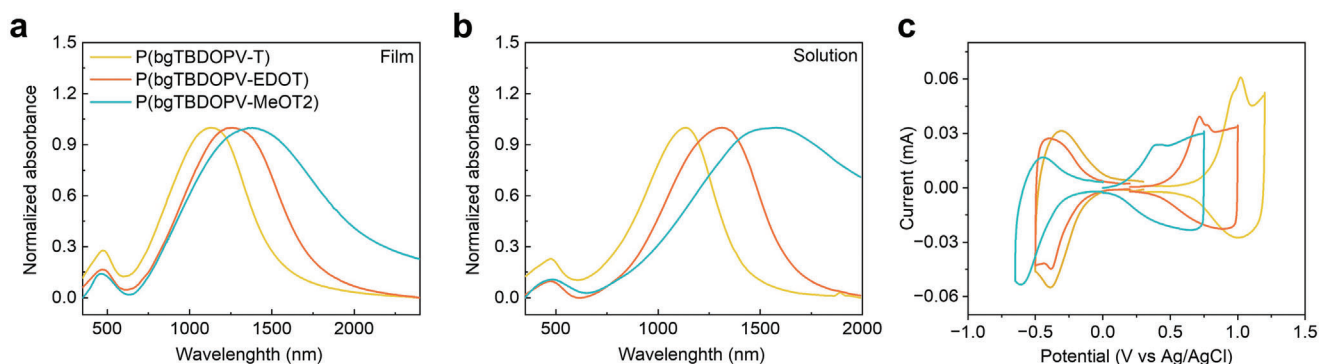


Figure 2. Normalized UV-vis-NIR absorption spectra of three polymers in a) film and b) HFIP solution. c) CV curves of the polymers with Fc/Fc^+ as the external standard.

P(bgTBDOPV-EDOT) and P(bgTBDOPV-MeOT2) exhibited low carrier injection barriers, resulting in reduced operating voltages with both p-type and n-type $|V_{Th}|$ values below 0.6 V. This advantage could reduce side reactions, enhance device stability, and support the development of low-power-consumption electronics.

The volumetric capacitance (C^*) of polymers was measured by electrochemical impedance spectroscopy (EIS) (Figure S5 and S6, Supporting Information). Compared with P(bgTBDOPV-MeOT2), P(bgTBDOPV-EDOT) exhibited higher C^* with p-type and n-type values of 150 and 218 $F\text{ cm}^{-3}$. The hole/electron mobility (μ) was calculated based on μC^* and C^* . The electron mobility of P(bgTBDOPV-EDOT) and P(bgTBDOPV-MeOT2) is 0.45 and 0.37 $\text{cm}^2\text{ V}^{-1}\text{ s}^{-1}$, respectively, representing high levels among n-type OECTs. The hole mobility exceeds the electron mobility, reaching 1.57 and 1.78 $\text{cm}^2\text{ V}^{-1}\text{ s}^{-1}$ for P(bgTBDOPV-EDOT) and P(bgTBDOPV-MeOT2), respectively. The above experiments demonstrate that using the strong proquinoidal TB-DOPV acceptor and adjusting the donor structures can achieve ambipolar OECT materials with excellent n-type and p-type performance.

We further measured the transient response of the ambipolar OECTs to evaluate the response times of three polymers. (Figure 3g; S12a,b, Supporting Information). P(bgTBDOPV-EDOT) and P(bgTBDOPV-MeOT2) exhibited short response times: $\tau_{on}/\tau_{off} = 0.48/0.36$ ms (p-type) and 0.41/0.41 ms (n-type) for P(bgTBDOPV-EDOT), and 0.49/0.37 ms (p-type) and 0.41/0.38 ms (n-type) for P(bgTBDOPV-MeOT2). The fast re-

sponse characteristics make these ambipolar OECTs promising for real-time high-speed sensing applications. We observed comparable on and off speeds for both polymers. The results were consistent across different devices, confirming their reliability (Figure S18, Supporting Information). However, in most accumulation-mode OECTs, the on speed is typically slower than the off. We tentatively attributed such phenomena to their minimal conformational changes during doping (Figure S16, Supporting Information), which has been reported as the primary reason for the on speed being slower than the off.^[26] However, due to the complexity of the factors affecting the OECT response, further studies are needed to elucidate the mechanism.

Continuous pulses were applied to the gate to evaluate operational stability during repeated switching (Figure 3h, Figure S12c,d, Supporting Information). After 200 on-off cycles over 400 s under ambient conditions, P(bgTBDOPV-EDOT) retained 81% (n-type) and 89% (p-type) of their initial on-current values, while P(bgTBDOPV-MeOT2) retained 90% for both n-type and p-type. The relatively poor p-type stability of P(bgTBDOPV-EDOT) is probably due to the weaker positive charge stabilization capability of EDOT compared to MeOT2 (Figure S17, Supporting Information).

Efficient logic circuits require both high-performance n-type and p-type transistors. We used the above ambipolar polymers as the channel material to construct inverter devices to demonstrate the potential of using ambipolar materials in constructing logic circuits (Figure S11, Supporting Information). An ideal inverter,

Table 1. OECT device performance of the three polymers.

	Type	$g_{m,norm}^a$ [$S\text{ cm}^{-1}$]	V_{Th}^b [V]	μC^{*c} [$F\text{ cm}^{-1}\text{ V}^{-1}\text{ s}^{-1}$]	μ^d [$\text{cm}^2\text{ V}^{-1}\text{ s}^{-1}$]	C^* [$F\text{ cm}^{-3}$]	τ_{on}/τ_{off} [ms]
P(bgTBDOPV-T)	p	75.6 ± 4.2	-0.72	349 ± 23	3.46	101 ± 6	0.99/0.44
	n	27.9 ± 1.6	0.26	84 ± 6	0.62	136 ± 2	0.38/0.31
P(bgTBDOPV-EDOT)	p	79.2 ± 4.4	-0.55	235 ± 16	1.57	150 ± 5	0.48/0.36
	n	31.0 ± 2.4	0.32	98 ± 9	0.45	218 ± 1	0.41/0.41
P(bgTBDOPV-MeOT2)	p	103 ± 4	-0.28	219 ± 11	1.78	123 ± 2	0.49/0.37
	n	19.4 ± 0.6	0.46	62 ± 3	0.37	167 ± 1	0.41/0.38

^{a)} The transconductance was normalized by the channel geometry. The W/L of all the devices is $100\text{ }\mu\text{m}/10\text{ }\mu\text{m}$. All the OECT devices were operated in a 0.1 M NaCl aqueous solution; ^{b)} V_{Th} was determined by extrapolating the corresponding $I_{DS}^{1/2}$ versus V_{GS} plot; ^{c)} μC^* was calculated according to Equation (1); ^{d)} μ was calculated from μC^* and the measured volumetric capacitance C^* . Five devices were tested and analyzed for each polymer (sample size $n = 5$). The values indicated after the “ \pm ” represent the standard deviation of the data.

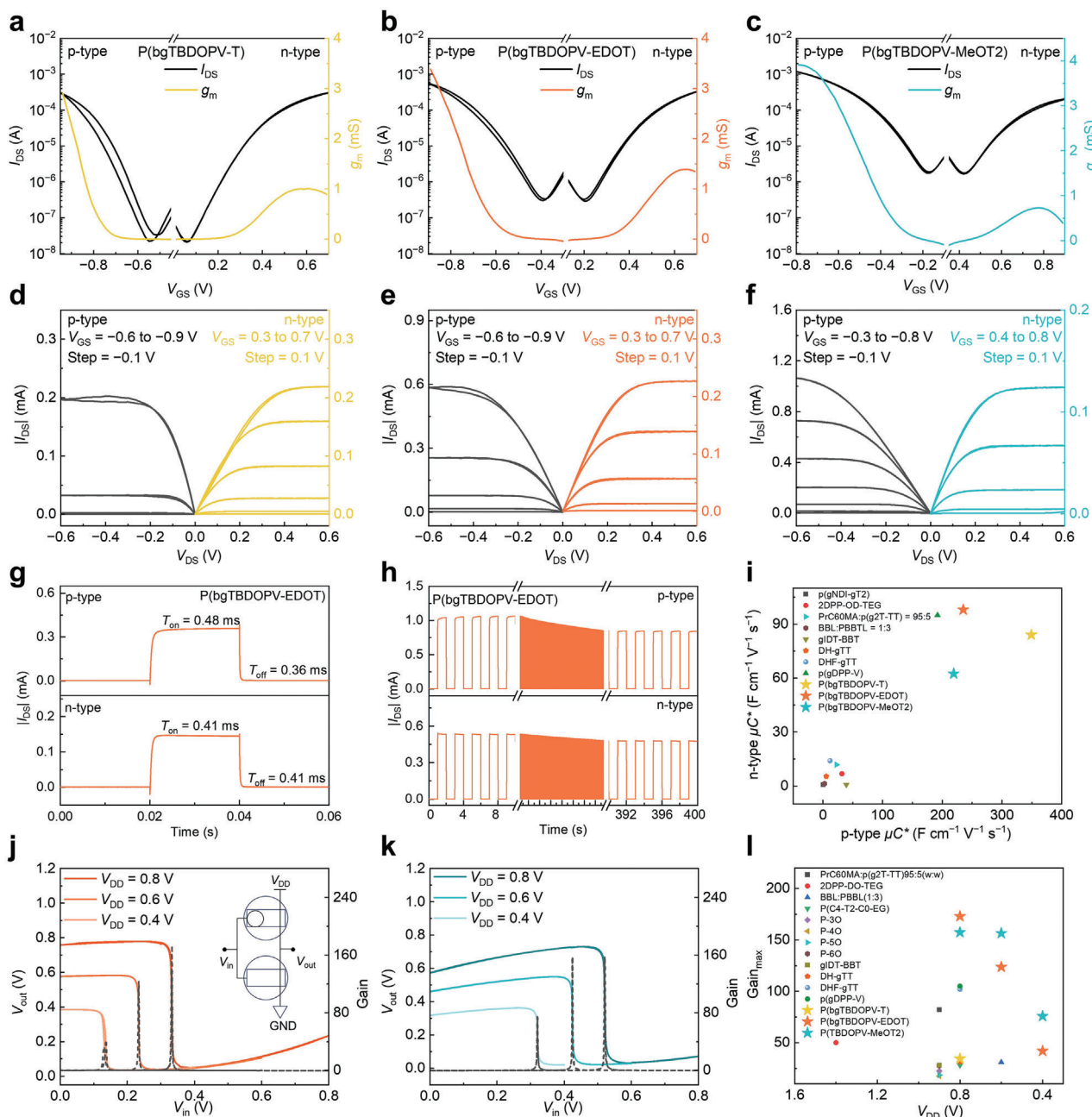


Figure 3. a–c) Transfer and d–f) output characteristics of OECTs based on P(bgTBDOPV-T), P(bgTBDOPV-EDOT), and P(bgTBDOPV-MeOT2). The transfer curves for p- and n-type OECTs were measured under the conditions of $V_{DS} = -0.6$ V and $V_{DS} = +0.6$ V, respectively. g) Transient on/off curves and h) operational stability of P(bgTBDOPV-EDOT)-based OECTs. On-state V_{GS} is the voltage at the maximum transconductance, while off-state V_{GS} is the voltage at the lowest current. The V_{DS} for p- and n-type OECTs were -0.6 V and $+0.6$ V, respectively. The operational stability test was conducted for 200 cycles over 400 s. i) Comparison of n -type and p -type μC^* values for P(bgTBDOPV-T), P(bgTBDOPV-EDOT), and P(bgTBDOPV-MeOT2)-based OECTs with other reported ambipolar OECTs.^[9,12–14,24] Voltage transfer characteristics and gain of the complementary inverters based on j) P(bgTBDOPV-EDOT) and k) P(bgTBDOPV-MeOT2). The scanning steps for the V_{in} are 0.5 mV. l) Summarized gain values of the inverters based on ambipolar OECTs in various V_{DD} .^[9,12,13,14b,16,24,25]

with well-matched n-type and p-type performance, should exhibit a stable voltage transfer characteristic (VTC) with a switching voltage at $V_{DD}/2$ and a sharp transition from V_{DD} to GND. This maximizes the noise margin (NM) and provides high gain during the sharp transition, enabling efficient on-site amplifi-

cation of biological signals.^[27] Due to the poor p-type stability of P(bgTBDOPV-T), the switching voltage of the inverter device decreased over time, resulting in an unstable VTC (Figure S13, Supporting Information). In contrast, the inverter based on P(bgTBDOPV-EDOT) showed a stable VTC with a switching

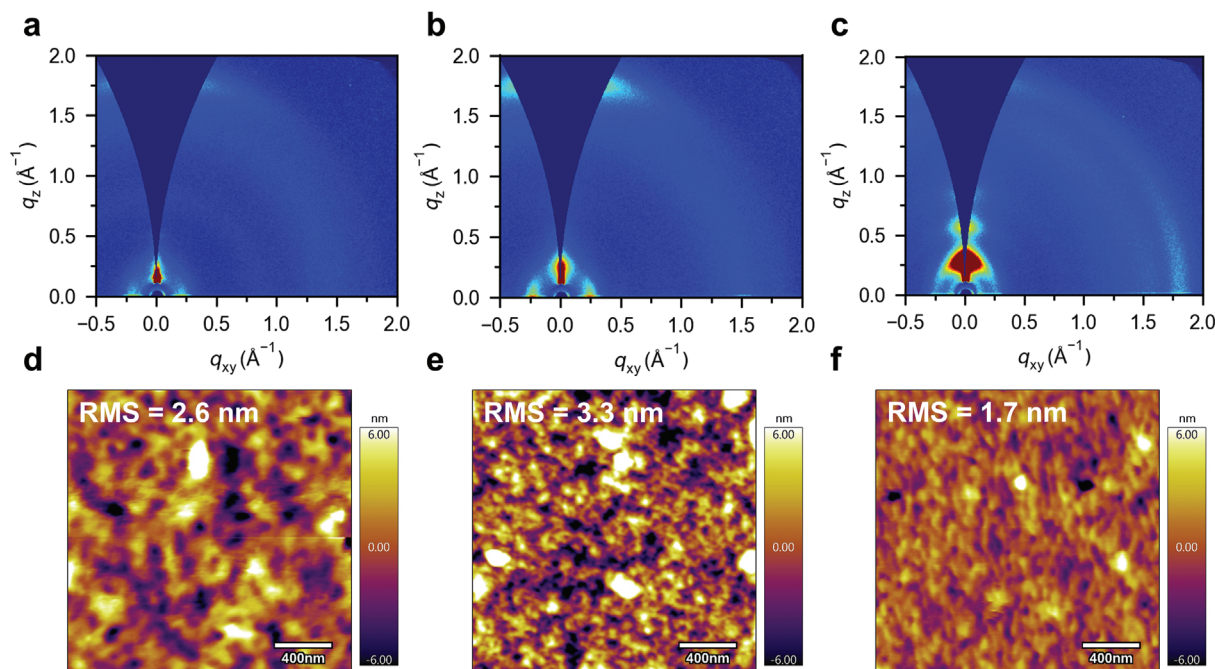


Figure 4. Molecular packing and morphology characterization. 2D-GIWAXS pattern of a) P(bgTBDOPV-T), b) P(bgTBDOPV-EDOT), and c) P(bgTBDOPV-MeOT2). AFM height images of d) P(bgTBDOPV-T), e) P(bgTBDOPV-EDOT), and f) P(bgTBDOPV-MeOT2) film. The scale bars are 400 nm. The film thicknesses are 80 nm.

voltage slightly lower than $V_{DD}/2$, indicating much more matched n-type and p-type performance. At $V_{DD} = 0.8$ V, the maximum gain at the output sharp transition reached 173 (Figure 3j). P(bgTBDOPV-MeOT2) also demonstrated a stable VTC. Due to its better p-type performance and suppressed n-type performance, the switching voltage is greater than $V_{DD}/2$, with a lower maximum gain of 157 (Figure 3k). Both P(bgTBDOPV-EDOT) and P(bgTBDOPV-MeOT2) exhibited the highest gain values for ambipolar OECT-based inverters reported to date (Figure 3l; Table S5, Supporting Information). Their stable VTCs and high gains highlight their potential for logic circuits and biosignal amplification. Notably, the low operating voltage characteristics of P(bgTBDOPV-EDOT) and P(bgTBDOPV-MeOT2) enable the construction of inverters with stable VTC and high gains even under low V_{DD} conditions. At $V_{DD} = 0.6$ V, P(bgTBDOPV-EDOT) and P(bgTBDOPV-MeOT2) achieved gains of 124 and 157, respectively. At $V_{DD} = 0.4$ V, they reached 42 and 76 (Figure 3l). This performance, which many other ambipolar materials cannot achieve, is desirable for low-power-consumption electronics.

2.3. Film Microstructures

The molecular packing and film morphology significantly influence the performance of semiconducting polymers. Thus, grazing incidence wide-angle X-ray scattering (GIWAXS) and atomic force microscope (AFM) were employed to examine these characteristics. P(bgTBDOPV-T) and P(bgTBDOPV-EDOT) displayed typical face-on molecular packing (Figure 4a,b). The smaller lamellar distance (d_{lam}) and increased lamellar coher-

ence length ($L_{c, lam}$) for P(bgTBDOPV-EDOT) suggest a more compact lamellar packing compared to P(bgTBDOPV-T) (Table S2, Supporting Information). Secondary bonding interactions between the oxygen atom in the EDOT fragment and the sulfur atom in the thiophene ring could enhance the conjugated backbone's planarity, as confirmed by the relaxed potential energy surface (PES) scan calculations (Figure S8b, Supporting Information). This increased planarity strengthens the interchain interactions, improving the order and crystallinity of P(bgTBDOPV-EDOT). Different from P(bgTBDOPV-T) and P(bgTBDOPV-EDOT), P(bgTBDOPV-MeOT2) exhibited typical edge-on molecular packing (Figure 4c) with the shortest π - π distance (3.48 Å), lamellar distance (22.9 Å), and maximum coherence lengths in both directions (Table S2, Supporting Information). We attribute the distinct packing and higher order in P(bgTBDOPV-MeOT2) to the centrosymmetric structure of the MeOT2 donor.^[28] The higher crystallinity may have contributed to the superior OECT operational stability of P(bgTBDOPV-EDOT) and P(bgTBDOPV-MeOT2) compared to P(bgTBDOPV-T).^[29] As revealed in the AFM height images (Figure 4d-f), all three polymer films showed very smooth surfaces, with root-mean-square (RMS) roughness values of 2.6, 3.3, and 1.7 nm, respectively.

2.4. Understanding the Strong Proquinoidal Design

To understand the impact of proquinoidal building blocks in constructing ambipolar OECTs, we compared several ambipolar OECT materials: P(gNDI-gT2),^[14a] DHF-gTT,^[16] P(bgTBDOPV-EDOT), and P(bgTBDOPV-MeOT2) (Figure 5a). All copolymers

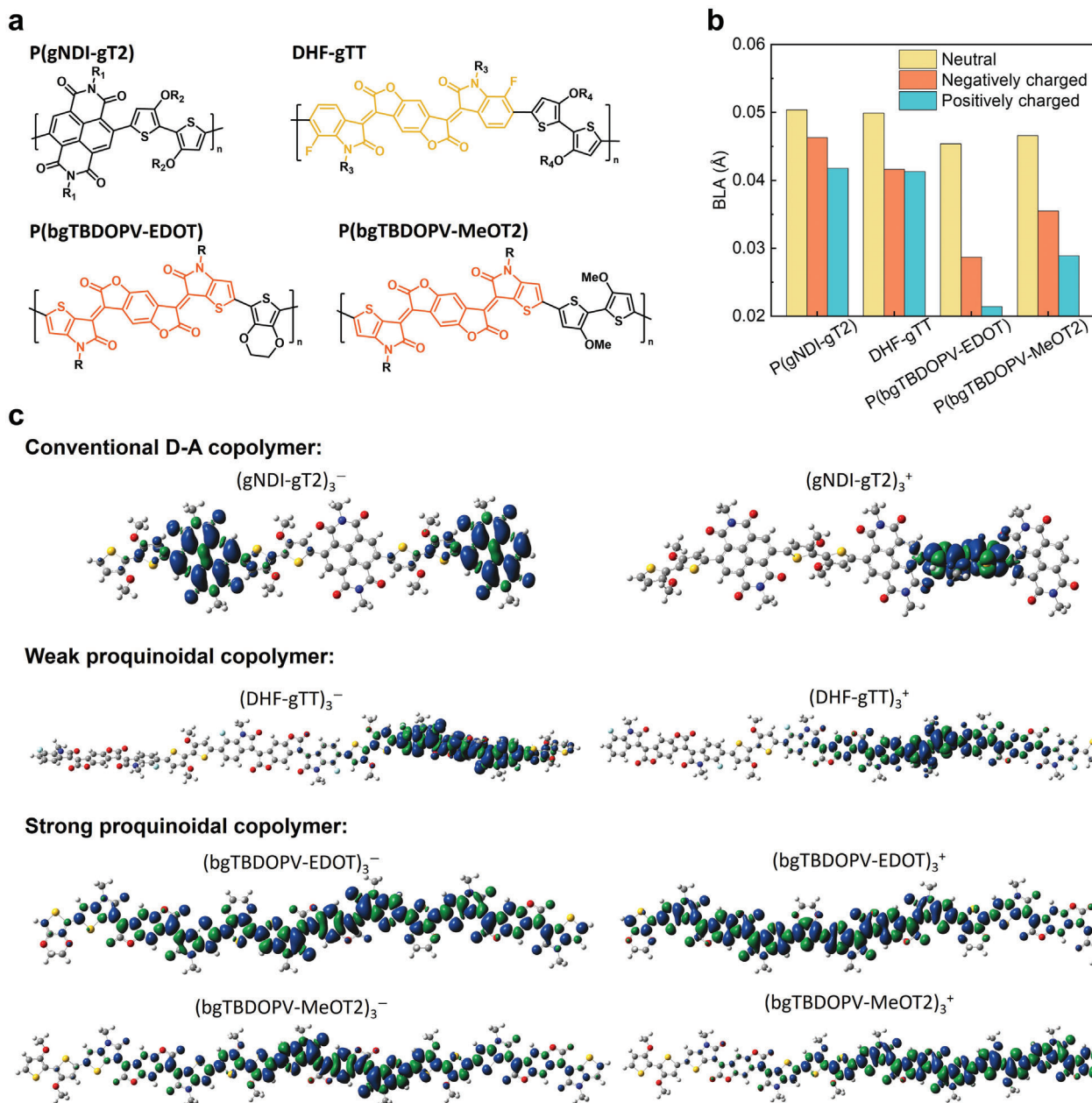


Figure 5. a) Chemical structures of four ambipolar polymers: P(gNDI-gT2), DHF-gTT, P(bgTBDOPV-EDOT), and P(bgTBDOPV-MeOT2). Different side chains are represented by R_{1-4} . P(gNDI-gT2) represents conventional D-A copolymer, DHF-gTT represents weak proquinoidal copolymer, while P(bgTBDOPV-EDOT) and P(bgTBDOPV-MeOT2) represent strong proquinoidal copolymers. b) BLAs and c) spin density distributions of four ambipolar polymers in negatively and positively charged states. Methyl groups are used to replace complex side-chain structures to simplify calculations.

have similar thiophene-based donors with different acceptors—NDI, BDOPV, and TBDOPV—which show progressively increasing ΔE_{ST} (Figure 1a), indicating enhanced proquinoidal characteristics. Performance improves significantly as the proquinoidal characteristics of the acceptors increase. The conventional D-A copolymer P(gNDI-gT2) shows p-type and n-type μC^* values below $1 \text{ F cm}^{-1} \text{ V}^{-1} \text{ s}^{-1}$. In contrast, the weak proquinoidal copolymer DHF-gTT and its derivative DH-gTT achieve μC^* values over $10 \text{ F cm}^{-1} \text{ V}^{-1} \text{ s}^{-1}$ (Table S4, Supporting Information). Our strong proquinoidal copolymers exhibited μC^* exceeding

$100 \text{ F cm}^{-1} \text{ V}^{-1} \text{ s}^{-1}$. These findings underscore the substantial impact of strong proquinoidal building blocks on the performance of ambipolar OECTs, motivating us to explore their underlying mechanisms.

Previous studies have shown that extensive polaron delocalization is crucial for achieving both high-performance p-type^[30] and n-type^[20,31] unipolar OECTs. In p-type materials, polythiophene-based all-donor polymers like PEDOT^[32] achieve high performance due to the alignment of the energy levels between adjacent segments, enabling widespread positive polaron

delocalization. In n-type materials, all-acceptor polymers like BBL^[33] demonstrate good n-type performance and excellent stability due to superior polaron delocalization. Incorporating electron-withdrawing groups into the donor segments of D-A copolymers to enhance negative polaron delocalization has become a crucial strategy for improving the performance of n-type materials.^[20,34] Leveraging unipolar material characteristics, we believe that enhancing the delocalization of both positive and negative polarons is essential for high-performance ambipolar OECT materials.

However, enhancing polaron delocalization poses challenges in developing high-performance ambipolar OECTs. All-donor and all-acceptor polymers typically exhibit large bandgaps, leading to either too-high or too-low energy levels of frontier orbitals to allow the effective injection of only one type of charge carrier. Researchers have attempted to construct narrow bandgap D-A copolymers^[14] using highly electron-rich donors and highly electron-deficient acceptors to enable the effective injection of both charge carriers, like P(gNDI-gT2). However, this significant energy level disparity results in positive polarons localizing in donors and negative polarons in acceptors, impairing charge transport. Strategies aimed at reducing the energy level difference to enhance polaron delocalization often increase bandgaps, resulting in unipolar behavior. For instance, our previous work demonstrated that introducing electron-withdrawing groups on donors can convert p-type materials into n-type materials, but without achieving ambipolarity.^[31] This analysis underscores the difficulty of reconciling narrow bandgaps with polaron delocalization in ambipolar OECT material design.

In contrast, the proquinoidal building blocks offer distinct advantages in constructing ambipolar materials. First, it inherently features a narrow bandgap (Figure S9, Supporting Information) that facilitates the injection of both electrons and holes,^[35] which also helps to reduce the operating voltages of ambipolar OECTs. More importantly, proquinoidal building blocks significantly enhance polaron delocalization. Polarons delocalization relies on the overlap of intramolecular and intermolecular wave functions of HOMO/LUMO. On one hand, the resonance between the quinoidal and aromatic forms promotes the intramolecular overlaps of HOMO and LUMO wavefunctions, allowing for greater delocalization of polarons within the molecule. On the other hand, quinoidal and aromatic resonances reduce torsional angles between adjacent segments and flatten the polymer backbone. This not only aids in polaron delocalization across the conjugated backbone but also enhances interchain π - π interactions, increasing the overlap of intermolecular frontier orbitals.^[36] Thus, the proquinoidal building blocks can promote the delocalization of both types of polarons while maintaining a narrow bandgap.

To validate these hypotheses, we conducted further DFT calculations. We calculated the bond length alternations (BLAs) for the ambipolar materials (Figure 5b; Figures S14 and S15, Supporting Information). The results indicate that polymers with strong proquinoidal acceptors, such as P(bgTBDOPV-EDOT) and P(bgTBDOPV-MeOT2), exhibit the lowest BLA values in both neutral and charged states, particularly when charged. The low BLA of P(bgTBDOPV-EDOT) and P(bgTBDOPV-MeOT2) in neutral states confirms the narrow bandgap characteristics of these materials and demonstrates their strong quinoidal character.^[37] Furthermore, the even lower BLA in charged states

suggests a greater tendency to form delocalized polarons, indicating a high-mobility character.^[38] Notably, P(bgTBDOPV-MeOT2) exhibits a slightly higher BLA than P(bgTBDOPV-EDOT), which explains its somewhat lower OECT performance.

As previously analyzed, achieving high ambipolar performance requires promoting the delocalization of both p-type and n-type polarons. Studies have shown that spin density distribution governs polaron delocalization.^[36a] We calculated the spin density distributions of the four polymers under their positively and negatively charged states (Figure 5c). In NDI polymers, positive polarons localize on donors and negative polarons on acceptors. In weak proquinoidal copolymers (BDOPV), polarons delocalize within a single repeat unit, while in strong proquinoidal copolymers (TBDOPV), both polarons delocalize over a broader range. These results demonstrate our hypothesis that the proquinoidal acceptors promote polarons delocalization, leading to improved OECT performance.

3. Conclusion

In conclusion, we have demonstrated that strong proquinoidal building blocks can enable narrow bandgaps and enhance the delocalization of both positive and negative polarons, effectively addressing the polaron localization issues of typical conventional D-A ambipolar OECT materials. By incorporating the strong proquinoidal acceptor, TBDOPV, we developed three high-performance ambipolar OECT materials, with P(bgTBDOPV-EDOT) exhibiting record-breaking performance, achieving a p-type μC^* of 268 F cm⁻¹ V⁻¹ s⁻¹ and an n-type μC^* of 107 F cm⁻¹ V⁻¹ s⁻¹. The normalized transconductance ($g_{m,norm}$) reached 88.3 and 34.8 S cm⁻¹, respectively. Additionally, P(bgTBDOPV-EDOT) operated at low voltages, and exhibited fast response times and excellent stability. As a channel material, P(bgTBDOPV-EDOT) enabled inverter devices with a high gain of 173 V/V and unprecedented capability to work under low voltages. Despite these advancements, challenges remain. The n-type regime performance lags behind the p-type regime, which is not balanced; the threshold voltages for both regimes are relatively large; and the device stability requires further improvement. Future research should focus on designing more diverse and robust proquinoidal building blocks and further exploring the structure-property relationships to achieve high-performance, stable, well-balanced ambipolar OECT materials. These advancements could significantly expand the application scope of ambipolar OECTs in next-generation electronics.

Supporting Information

Supporting Information is available from the Wiley Online Library or from the author.

Acknowledgements

This work is supported by the National Key R&D Program of China (2024YFF0509300), the National Natural Science Foundation of China (T2425010), and the Beijing Natural Science Foundation (JQ22006). The authors acknowledge Molecular Materials and Nanofabrication Laboratory (MMNL) and Materials Processing and Analysis Center, Peking University, for the use of instruments. The computational part is supported by

the High-Performance Computing Platform of Peking University. The authors thank beamline BL14B1 (Shanghai Synchrotron Radiation Facility) for providing beam time.

Conflict of Interest

The authors declare no competing financial or non-financial interests.

Author Contributions

X.P. and Z.R. contributed equally to this work. Z.R., X.P., J.-P.C., G.-Y.G., Q.L., and Z.X. synthesized the polymers. X.P., Y.C., Y.Z., P.L., W.S., and J.X. performed device fabrication and characterization. X.P. performed DFT calculations. X.P., Z.R., Z.Z., R.Z., Y.-Q.Z., and T.L. wrote the manuscript. All the authors revised and approved the manuscript.

Data Availability Statement

The data that support the findings of this study are available from the corresponding author upon reasonable request.

Keywords

ambipolarity, inverters, organic electrochemical transistors, proquinoidal building blocks

Received: November 6, 2024
Revised: January 26, 2025
Published online:

- [1] a) A. Koklu, D. Ohayon, S. Wustoni, V. Druet, A. Saleh, S. Inal, *Chem. Rev.* **2022**, *122*, 4581; b) H. Kim, Y. Won, H. W. Song, Y. Kwon, M. Jun, J. H. Oh, *Adv. Sci.* **2024**, *11*, 2306191.
- [2] Y. Zhong, A. Saleh, S. Inal, *Macromol. Biosci.* **2021**, *21*, 2100187.
- [3] P. Gkoupidenis, Y. Zhang, H. Kleemann, H. Ling, F. Santoro, S. Fabiano, A. Salleo, Y. van de Burgt, *Nat. Rev. Mater.* **2024**, *9*, 134.
- [4] a) J. Rivnay, S. Inal, A. Salleo, R. M. Owens, M. Berggren, G. G. Malliaras, *Nat. Rev. Mater.* **2018**, *3*, 17086; b) E. Zeglio, O. Inganäs, *Adv. Mater.* **2018**, *30*, 1800941.
- [5] P. Romele, P. Gkoupidenis, D. A. Koutsouras, K. Lieberth, Z. M. Kovács-Vajna, P. W. M. Blom, F. Torricelli, *Nat. Commun.* **2020**, *11*, 3743.
- [6] P. Li, W. Sun, J. Li, J.-P. Chen, X. Wang, Z. Mei, G. Jin, Y. Lei, R. Xin, M. Yang, J. Xu, X. Pan, C. Song, X.-Y. Deng, X. Lei, K. Liu, X. Wang, Y. Zheng, J. Zhu, S. Lv, Z. Zhang, X. Dai, T. Lei, *Science* **2024**, *384*, 557.
- [7] I. Uguz, D. Ohayon, S. Yilmaz, S. Griggs, R. Sheelamantula, J. D. Fabbri, I. McCulloch, S. Inal, K. L. Shepard, *Sci. Adv.* **2024**, *10*, eadi9710.
- [8] P. C. Harikesh, C.-Y. Yang, D. Tu, J. Y. Gerasimov, A. M. Dar, A. Armada-Moreira, M. Massetti, R. Kroon, D. Bliman, R. Olsson, E. Stavrinidou, M. Berggren, S. Fabiano, *Nat. Commun.* **2022**, *13*, 901.
- [9] J. J. Samuel, A. Garudapalli, A. A. Mohapatra, C. Gangadharappa, S. Patil, N. P. B. Aetukuri, *Adv. Funct. Mater.* **2021**, *31*, 2102903.
- [10] Y. Ren, X. Yang, L. Zhou, J. Y. Mao, S. T. Han, Y. Zhou, *Adv. Funct. Mater.* **2019**, *29*, 1902105.
- [11] R. B. Rashid, W. Du, S. Griggs, I. P. Maria, I. McCulloch, J. Rivnay, *Sci. Adv.* **2021**, *7*, eabh1055.
- [12] S. Cong, J. Chen, M. Xie, Z. Deng, C. Chen, R. Liu, J. Duan, X. Zhu, Z. Li, Y. Cheng, W. Huang, I. McCulloch, W. Yue, *Sci. Adv.* **2024**, *10*, eadq9405.
- [13] E. Stein, O. Nahor, M. Stolov, V. Freger, I. M. Petruta, I. McCulloch, G. L. Frey, *Nat. Commun.* **2022**, *13*, 5548.
- [14] a) A. Giovannitti, C. B. Nielsen, D. T. Sbircea, S. Inal, M. Donahue, M. R. Niazi, D. A. Hanifi, A. Amassian, G. G. Malliaras, J. Rivnay, I. McCulloch, *Nat. Commun.* **2016**, *7*, 13066; b) D. Ohayon, A. Savva, W. Du, B. D. Paulsen, I. Uguz, R. S. Ashraf, J. Rivnay, I. McCulloch, S. Inal, *ACS Appl. Mater. Interfaces.* **2021**, *13*, 4253; c) Y. Zhang, G. Ye, T. P. A. van der Pol, J. Dong, E. R. W. van Doremaele, I. Krauhausen, Y. Liu, P. Gkoupidenis, G. Portale, J. Song, R. C. Chiechi, Y. van de Burgt, *Adv. Funct. Mater.* **2022**, *32*, 2201593.
- [15] a) A. Giovannitti, R. B. Rashid, Q. Thiburce, B. D. Paulsen, C. Cendra, K. Thorley, D. Moia, J. T. Mefford, D. Hanifi, D. Weiyuan, M. Moser, A. Salleo, J. Nelson, I. McCulloch, J. Rivnay, *Adv. Mater.* **2020**, *32*, 1908047; b) R. Ding, X. Zhang, R. Yan, M. Peng, S. Su, S. Y. Jeong, H. Y. Woo, X. Guo, K. Feng, Z.-H. Guo, *Adv. Funct. Mater.* **2024**, *35*, 2412181.
- [16] G. Qi, M. Wang, S. Wang, S. Zhang, X. Teng, H. Bai, B. Wang, C. Zhao, W. Su, Q. Fan, W. Ma, *Adv. Funct. Mater.* **2024**, *35*, 2413112.
- [17] Y. Cao, J.-H. Dou, N. Zhao, S. Zhang, Y.-Q. Zheng, J.-P. Zhang, J.-Y. Wang, J. Pei, Y. Wang, *Chem. Mater.* **2017**, *29*, 718.
- [18] a) R. Vargas, M. Galván, A. Vela, *J. Phys. Chem. A* **1998**, *102*, 3134; b) X. X. Chen, J. T. Li, Y. H. Fang, X. Y. Deng, X. Q. Wang, G. Liu, Y. Wang, X. Gu, S. D. Jiang, T. Lei, *Nat. Commun.* **2022**, *13*, 2258.
- [19] a) Z. Chen, W. Li, M. A. Sabuj, Y. Li, W. Zhu, M. Zeng, C. S. Sarap, M. M. Huda, X. Qiao, X. Peng, D. Ma, Y. Ma, N. Rai, F. Huang, *Nat. Commun.* **2021**, *12*, 5889; b) Z. Sun, Q. Ye, C. Chi, J. Wu, *Chem. Soc. Rev.* **2012**, *41*, 7857.
- [20] J. Shi, P. Li, X.-Y. Deng, J. Xu, Z. Huang, Y. Lei, Y. Wang, J.-Y. Wang, X. Gu, T. Lei, *Chem. Mater.* **2022**, *34*, 864.
- [21] F. Hu, Y. Xue, N. Jian, K. Qu, K. Lin, X. Zhu, T. Wu, X. Liu, J. Xu, B. Lu, *Electrochim. Acta.* **2020**, *357*, 136859.
- [22] H. Jia, Z. Huang, P. Li, S. Zhang, Y. Wang, J.-Y. Wang, X. Gu, T. Lei, *J. Mater. Chem. C* **2021**, *9*, 4927.
- [23] D. A. Bernards, G. G. Malliaras, *Adv. Funct. Mater.* **2007**, *17*, 3538.
- [24] a) X. Wu, T. L. D. Tam, S. Chen, T. Salim, X. Zhao, Z. Zhou, M. Lin, J. Xu, Y.-L. Loo, W. L. Leong, *Adv. Mater.* **2022**, *34*, 2206118; b) Y. Sun, Y. Lan, M. Li, W. Feng, M. Xie, Y. Lai, W. Li, Y. Cheng, J. Chen, W. Huang, L.-W. Feng, J. Ding, *Aggregate* **2024**, *5*, e577.
- [25] T. Pan, X. Jiang, E. R. W. van Doremaele, J. Li, T. P. A. van der Pol, C. Yan, G. Ye, J. Liu, W. Hong, R. C. Chiechi, Y. de Burgt, Y. Zhang, *Adv. Sci.* **2024**, *11*, 2400872.
- [26] J. Guo, S. E. Chen, R. Giridharagopal, C. G. Bischak, J. W. Onorato, K. Yan, Z. Shen, C.-Z. Li, C. K. Luscombe, D. S. Ginger, *Nat. Mater.* **2024**, *23*, 656.
- [27] M. Braendlein, T. Lonjaret, P. Leleux, J.-M. Badier, G. G. Malliaras, *Adv. Sci.* **2017**, *4*, 1600247.
- [28] T. Lei, Y. Cao, X. Zhou, Y. Peng, J. Bian, J. Pei, *Chem. Mater.* **2012**, *24*, 1762.
- [29] S.-M. Kim, C.-H. Kim, Y. Kim, N. Kim, W.-J. Lee, E.-H. Lee, D. Kim, S. Park, K. Lee, J. Rivnay, M.-H. Yoon, *Nat. Commun.* **2018**, *9*, 3858.
- [30] M. Moser, A. Savva, K. Thorley, B. D. Paulsen, T. C. Hidalgo, D. Ohayon, H. Chen, A. Giovannitti, A. Marks, N. Gasparini, A. Wadsworth, J. Rivnay, S. Inal, I. McCulloch, *Angew. Chem. Int. Ed. Engl.* **2021**, *60*, 7777.
- [31] P. Li, J. Shi, Y. Lei, Z. Huang, T. Lei, *Nat. Commun.* **2022**, *13*, 5970.
- [32] M. J. Donahue, A. Sanchez-Sanchez, S. Inal, J. Qu, R. M. Owens, D. Mecerreyes, G. G. Malliaras, D. C. Martin, *Mater. Sci. Eng. R Rep.* **2020**, *140*, 100546.
- [33] H. Y. Wu, C. Y. Yang, Q. Li, N. B. Kolhe, X. Strakosas, M. A. Stoessel, Z. Wu, W. Jin, M. Savvakis, R. Kroon, D. Tu, H. Y. Woo, M. Berggren, S. A. Jenekhe, S. Fabiano, *Adv. Mater.* **2022**, *34*, 2106235.

- [34] K. Feng, W. Shan, J. Wang, J.-W. Lee, W. Yang, W. Wu, Y. Wang, B. J. Kim, X. Guo, H. Guo, *Adv. Mater.* **2022**, *34*, 2201340.
- [35] T. Mikie, I. Osaka, *J. Mater. Chem. C* **2020**, *8*, 14262.
- [36] a) T. L. Dexter Tam, A. Moudgil, W. J. Teh, Z. M. Wong, A. D. Handoko, S. W. Chien, S.-W. Yang, B. S. Yeo, W. L. Leong, J. Xu, *J. Phys. Chem. B.* **2022**, *126*, 2073; b) T. Mikie, M. Hayakawa, K. Okamoto, K. Iguchi, S. Yashiro, T. Koganezawa, M. Sumiya, H. Ishii, S. Yamaguchi, A. Fukazawa, I. Osaka, *Chem. Mater.* **2021**, *33*, 8183; c) R. Wu, Y. Wei, X. Dai, L. Yan, W. Liu, D. Yuan, J. Zhu, X. Zhu, *Angew. Chem., Int. Ed.* **2024**, *64*, 202413061. d) X. Ji, L. Fang, *Polym. Chem.* **2021**, *12*, 1347.
- [37] J. L. Brédas, *J. Chem. Phys.* **1985**, *82*, 3808.
- [38] B. Yuan, C. Li, Y. Zhao, O. Gröning, X. Zhou, P. Zhang, D. Guan, Y. Li, H. Zheng, C. Liu, Y. Mai, P. Liu, W. Ji, J. Jia, S. Wang, *J. Am. Chem. Soc.* **2020**, *142*, 10034.